Elastic Interaction between a Vortex Dipole and an Axisymmetrical Vortex in Two-Dimensional Flows

V. Zoeller[1], **A. Viúdez**[1]

[1]Department of Physical Oceanography and Technology, Institute of Marine Sciences, CSIC, Barcelona 08003, Spain

Key Points:

- Numerical description of an elastic interaction between a Lamb-Chaplygin dipole and an axisymmetrical vortex in two-dimensional flows
- Numerical simulations of inelastic interactions with vortex partner exchange, merging and straining out processes
- Results are applicable to three-dimensional baroclinic geophysical flows under the quasi-geostrophic approximation

Corresponding author: Victoria Zoeller, `zoeller@icm.csic.es`

Abstract

We investigate numerically the elastic interaction between a dipole and an axisymmetrical vortex in inviscid isochoric two-dimensional flows satisfying Euler's vorticity conservation equation. This work contributes to previous studies addressing inelastic vortex interactions. The dipole is a straight moving Lamb-Chaplygin (L-C) vortex, where the absolute value of either the positive or the negative amount of vorticity equals the amount of vorticity of the target vortex. The results show that, when the straight moving L-C dipole approaches the axisymmetrical vortex, the potential flows of both vortices interact, the dipole's trajectory acquires curvature and the dipole's vorticity poles separate. Once the L-C dipole moves away from the target vortex, the poles close and the dipole continues with a straight trajectory but along a direction different from the initial one. Though there is very small vorticity exchange between the dipole's poles and a small vorticity leakage to the background field, the vortices preserve, to a large extent, their amount of vorticity and the resulting interaction may be practically qualified as an elastic interaction. This process is sensitive to the initial conditions and, depending on the initial position of the dipole as well as on small changes in the vorticity distribution of the axisymmetrical vortex, inelastic interactions may instead occur. Since the initial vorticity distributions are based on the eigenfunctions of the two-dimensional Laplacian operator in circular geometry these results are directly applicable to three-dimensional baroclinic geophysical flows under the quasi-geostrophic approximation.

Plain Language Summary

Ocean swirls, also known as eddies or vortices are ubiquitous in all oceans. Often they drift as two vortices together, rotating in opposite direction, known as eddy-pairs. The eddy-pair can encounter with different structures as well as with other ocean vortices. Here we prove that elastic interaction between two vortices are possible, meaning that the interaction does not change the vorticity properties of the vortices. We also describe numerically inelastic interactions, where the dipole (vortex-pair) separates or looses part of its vorticity. We use a two-dimensional model as many geophysical ocean processes occur on an approximately horizontal scale, though we show that the results given are also applicable to three-dimensional baroclinic flows.

1 Introduction

Mesoscale and submesoscale vortical structures are ubiquitous in the oceans and atmosphere. In particular, cyclonic and anticylonic vortices are found in different configurations, including monopoles, dipoles, and tripoles. Specifically, vortex dipoles, also known as vortex pairs or couples, double vortices, modons, or mushroom-like vortices have been observed all over the oceans. Some examples include vortex pairs of the southern coast of Madagascar (de Ruijter et al., 2004; Ridderinkhof et al., 2013), eastern of Australia (Li et al., 2020), the Norwegian coast (Johannessen et al., 1989), the Mexican coast (Santiago-García et al., 2019), California coast (Sheres & Kenyon, 1989), in the Alaska current (Ahlnäs et al., 1987), in the South China Sea (Huang et al., 2017) and along the Canary Islands (Barton et al., 2004). These dipoles are generated by different causes, including the instability of baroclinic currents (Carton, 2001), localized forcing in a viscous stratified fluid (Voropayev & Afanasyev, 1994), or coastal interaction (de Ruijter et al., 2004).

The dipole structure and its stability has been subject of many experimental, laboratory, and numerical studies (Couder & Basdevant, 1986; Flór & Van Heijst, 1994; Rasmussen et al., 1996; Voropayev & Afanasyev, 1994). The dipole possesses a propagation speed, and may be considered as the simplest self-induced translating vortex structure (Afanasyev, 2003; Carton, 2001). For this reason it can interact with, for example, a sloping boundary (Kloosterziel et al., 1993), a submarine mountain (Zavala Sansón & Gonzalez, 2021), a coastline (de Ruijter et al., 2004), inertia–gravity waves (Claret & Viúdez, 2010; Huang et al., 2017), other dipoles (Afanasyev, 2003; Dubosq & Viúdez, 2007; McWilliams & Zabusky, 1982; Velasco Fuentes & Heijst, van, 1995; Voropayev & Afanasyev, 1992) or other multipolar vortices (Besse et al., 2014; Viúdez, 2021; Voropayev & Afanasyev, 1992). Most of these interactions seem to be inelastic, in the sense that the vorticity dipole suffers irreversible changes during the interaction, for example during vortex merging or partial or complete straining out processes (Dritschel, 1995; Dritschel & Waugh, 1992; Dubosq & Viúdez, 2007; McWilliams & Zabusky, 1982; Voropayev & Afanasyev, 1992). However, in many instances ocean vortices do not interact strongly with one another for long time periods (Carton, 2001). Consequently, elastic interactions, where vorticity exchange does not occur, are also possible between ocean vortices. In this study we investigate numerically, as a particular kind of elastic dipole-vortex interaction, the interaction between a translating dipole and an axisymmetrical vortex.

In view of the complexity of baroclinic three-dimensional (3D) vortices, it is more practical to investigate first the barotropic two-dimensional (2D) case, assuming an adiabatic, inviscid, and incompressible fluid, satisfying the Euler equation of motion, which in this case reduces to the material conservation of vertical vorticity $\zeta(\mathbf{x},t) \equiv \mathbf{k}\cdot\nabla\times\mathbf{u}(\mathbf{x},t)$, where $\mathbf{u}(\mathbf{x},t)$ is the horizontal velocity field, ∇ is the 2D gradient operator and $\mathbf{k}$ is the vertical unit vector. Many geophysical processes occur on approximately horizontal scales, where the vertical, gravity oriented, velocity component is several orders of magnitude smaller than the horizontal velocity component (Wayne, 2011). For example, in the case of dipole-dipole interactions, Dubosq and Viúdez (2007) investigated numerically non-axial frontal collisions of mesoscale baroclinic dipoles as well as 2D dipole collisions, and concluded that the 3D inelastic interaction processes were qualitatively similar to the 2D interactions, as long as, the vortices had a similar vertical extent. In this study, where we deal with elastic interactions, the two-dimensional processes are expected to be dominant. Our aim here is to understand the 2D dynamics of elastic interactions, as a first step to correctly understand the more complicated 3D elastic interactions of balanced, that is in absence of inertia–gravity waves, flows.

The basic fluid dynamic equations, leading to the material conservation of vertical vorticity, are briefly introduced in section 2. In the following section 3, the initial vorticity conditions are explained. The dipole model used is based on the two-dimensional Lamb-Chaplygin (L-C) dipole (Chaplygin, 2007), which is an exact theoretical dipole model that translates rigid and straight with constant speed, while the target vortex has a radial vorticity distribution given by the Bessel function of 0-order $\mathrm{J}_0(r)$. In the next step, section 4, we describe numerical results showing that the dipole may be scattered by vortices, changing drastically its direction without modifying its vorticity distribution significantly, making possible elastic interactions. Finally concluding remarks are given in section 5.

2 Basic Equations

In 2D isochoric flows the stream function $\psi(\mathbf{x},t)$ provides the horizontal velocity $\mathbf{u}(\mathbf{x},t)$

$$\mathbf{u} \equiv -\nabla\times(\psi\mathbf{k})\,, \tag{1}$$

and vertical vorticity $\zeta(\mathbf{x},t)$

$$\zeta \equiv \mathbf{k}\cdot\nabla\times\mathbf{u} = \nabla^2\psi\,, \tag{2}$$

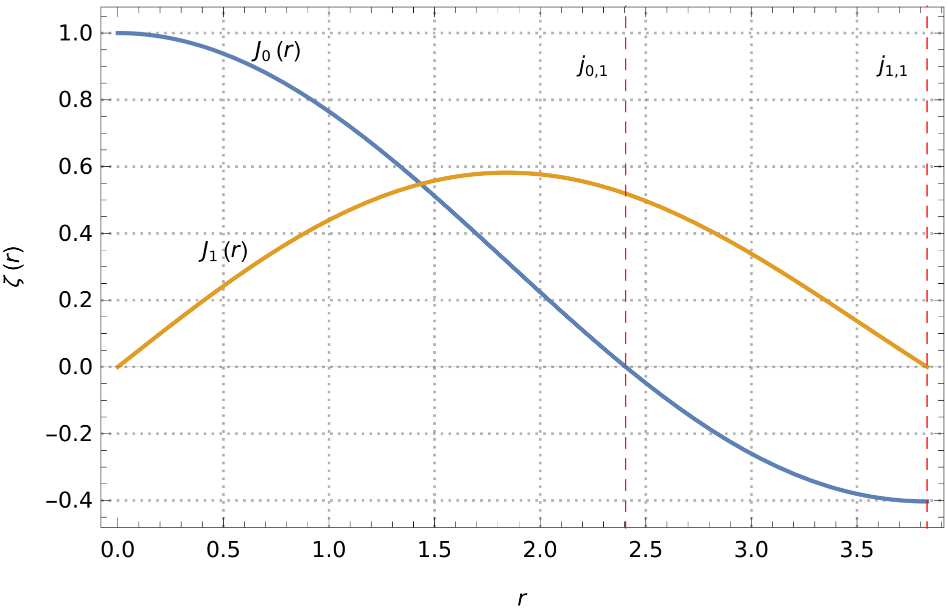

Figure 1. Bessel functions $\mathrm{J}_0(r)$ (blue) and $\mathrm{J}_1(r)$ (yellow). The red line stands for the zeroes $j_{0,1}$ and $j_{1,1}$

where $\mathbf{k}$ is the vertical unit vector and ∇ is the 2D gradient operator. The basic dynamical equation is the material conservation of vorticity

$$\frac{d\zeta}{dt} \equiv \frac{\partial \zeta}{\partial t} + \mathbf{u} \cdot \nabla \zeta = 0\,. \tag{3}$$

Equation (3) is numerically integrated (a brief description is given in Appendix A) to evolve in time the vorticity field from the initial vorticity conditions described in the next section.

3 Initial Conditions: Lamb-Chaplygin Dipole and Axisymmetrical Vortex

We use the Lamb-Chaplygin dipole model whose vorticity distribution $\zeta_d(r,\theta)$ in polar coordinates (r,θ) is a piecewise function given by

$$\zeta_d(r,\theta) \equiv \begin{cases} C_d \mathrm{J}_1(k_1 r)\sin\theta & 0 \le k_1 r \le j_{1,1} \\ 0 & j_{1,1} < k_1 r \end{cases}, \tag{4}$$

where C_d is a constant vorticity amplitude, $\mathrm{J}_m(r)$ is the Bessel function of order m, $j_{m,n}$ is the nth zero of $\mathrm{J}_m(r)$ (Figure 1) and k_1 is the dipole's wavenumber. This dipole moves, in absence of background velocity, straight along the x-axis with a constant speed equal to $u_0 = -C_d \mathrm{J}_0(j_{1,1})/(2k_1)$. The interior and exterior velocity fields $\mathbf{u}_d(r,\theta)$, in polar coordinates, are given by

$$\frac{\mathbf{u}_d(r,\theta)}{C_d/k_1} \equiv \begin{cases} \frac{\mathrm{J}_1(k_1 r)}{k_1 r}\cos\theta\,\mathbf{e}_r - \frac{1}{2}\left(\mathrm{J}_0(k_1 r) - \mathrm{J}_2(k_1 r)\right)\sin\theta\,\mathbf{e}_\theta & 0 \le k_1 r \le j_{1,1} \\ \frac{\mathrm{J}_0(j_{1,1})}{2k_1^2 r^2}\left[(k_1^2 r^2 - j_{1,1}^2)\cos\theta\,\mathbf{e}_r - (k_1^2 r^2 + j_{1,1}^2)\sin\theta\,\mathbf{e}_\theta\right] & j_{1,1} < k_1 r \end{cases}, \tag{5}$$

where $\mathbf{e}_r$ and $\mathbf{e}_\theta$ are the radial and azimuthal unit basis vectors.

In order to provide flow solutions with vanishing velocity at infinity we must add to the steady piecewise flow (5) a background flow $\mathbf{u}_0(\mathbf{x})$, applied to the complete spatial domain, such that the exterior velocity $\mathbf{u}_d(r,\theta) \to \mathbf{0}$ as $kr \to \infty$. The new solutions are time dependent and in Cartesian coordinates (x, y) are expressed as follows

$$\bar{\mathbf{u}}_d(x,y,t) \equiv \mathbf{u}_d(r(x-u_0t,y),\theta(x-u_0t,y)) + u_0\mathbf{e}_r\,, \tag{6}$$

where $\mathbf{u}_d(r,\theta)$ is the velocity field (5) in the steady state, $r(x,y) = \sqrt{x^2+y^2}$ and $\theta(x,y) = \arctan(y/x)$.

The vorticity distribution $\zeta_v(r,\theta)$ of the axisymmetrical vortex is given by the Bessel function of order 0 (Figure 1), truncated at a radius $r = j_{0,1}/k_2$, that is

$$\zeta_v(r,\theta) \equiv \begin{cases} C_v \mathrm{J}_0(k_2 r) & 0 \le k_2 r \le j_{0,1} \\ 0 & j_{0,1} < k_2 r \end{cases}\,, \tag{7}$$

where C_v is a constant vorticity amplitude and k_2 is the vortex's wavenumber. The vortex velocity $\mathbf{u}_v(r) = v(r)\mathbf{e}_\theta$ is azimuthal and is given by

$$\frac{v(r)}{C_v/k_2} \equiv \begin{cases} \mathrm{J}_1(k_2 r) & 0 \le k_2 r \le j_{0,1} \\ \frac{\mathrm{J}_1(j_{0,1})j_{0,1}}{k_2 r} & j_{0,1} < k_2 r \end{cases}\,. \tag{8}$$

When both, vortex and dipole, are present they interact due to their exterior potential flows. This interaction depends on the vortices amplitude (C_d, C_v) and vortices extension given by the wavenumbers (k_1, k_2). We are interested in interactions between vortices with equal size and amplitude and therefore we set the positive circulation of the dipole (Γ_d^+) equal to the circulation of the vortex (Γ_v^+), and the area of the vortex (A_v) equal to the area of the positive vorticity of the dipole (A_d^+), that is

$$\Gamma_d^+ = \Gamma_v^+\,, \quad A_d^+ = A_v\,. \tag{9}$$

The radius of the vortex is $R_v = j_{0,1}/k_2$, which implies $A_v = \pi(j_{0,1}/k_2)^2$. Since the radius of the dipole is $R_d = j_{1,1}/k_1$, the area is $A_d^+ = \pi(j_{1,1}/k_1)^2/2$ and applying (9), we obtain the wavenumber ratio

$$\frac{k_1}{k_2} = \frac{1}{\sqrt{2}}\frac{j_{1,1}}{j_{0,1}} \simeq 1.127\,. \tag{10}$$

The amplitudes ratio C_v/C_d is obtained from the circulation of the vortex and the positive part of the dipole. The positive circulation of the dipole is

$$\frac{\Gamma_d^+}{C_d} = \int_0^\pi \sin\theta\, d\theta \int_0^{j_{1,1}/k_1} \mathrm{J}_1(k_1 r)\, r\, dr = -\frac{\pi}{k_1^2} j_{1,1} \mathrm{H}_1(j_{1,1}) \mathrm{J}_0(j_{1,1})\,, \tag{11}$$

where $\mathrm{H}_1(x)$ is the Struve function of order 1. The circulation of the vortex is

$$\frac{\Gamma_v^+}{C_v} = \int_0^{2\pi} d\theta \int_0^{j_{0,1}/k_2} \mathrm{J}_0(k_2 r)\, r\, dr = \frac{2\pi}{k_2^2} j_{0,1} \mathrm{J}_1(j_{0,1})\,, \tag{12}$$

and therefore applying (9) we obtain the vorticity amplitudes ratio

$$\frac{C_d}{C_v} = -\frac{j_{1,1}\mathrm{J}_1(j_{0,1})}{\mathrm{H}_1(j_{1,1})\mathrm{J}_0(j_{1,1})j_{0,1}} \simeq 1.889\,. \tag{13}$$

The initial vorticity distribution is represented in figure 2. The dipole's poles are close together and have the same vorticity contours as the axisymmetrical vortex. The initial interaction between both vortices, as inferred from the stream function is negligible. This initial vorticity distribution is integrated in time following the steps explained in Appendix A. In the next section, we describe the numerical results of the elastic interaction between both vortices.

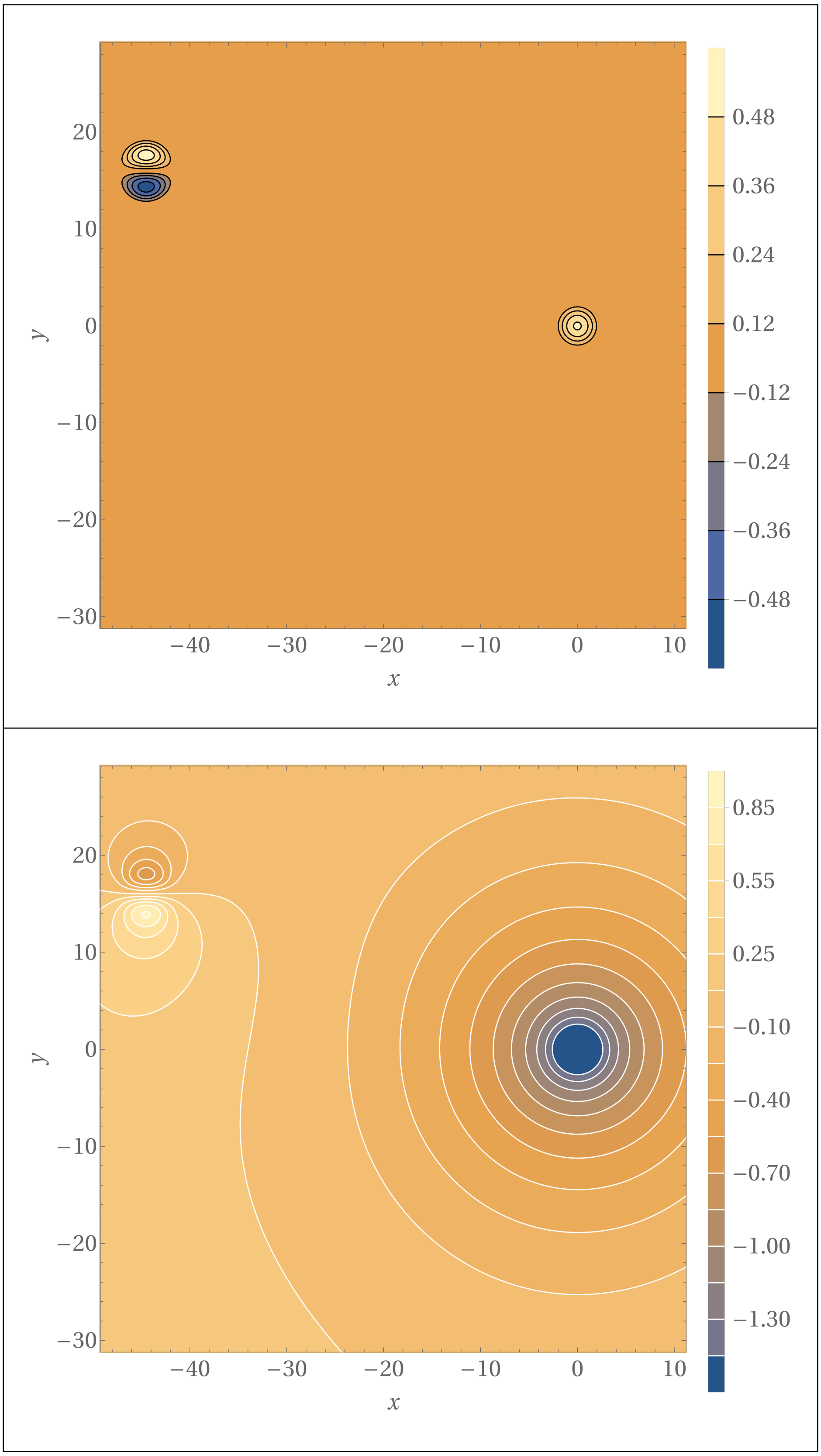

Figure 2. Vorticity (top) and stream function (bottom) distributions at $t = 0$.

4 Numerical Results

This section analyses numerically the interaction between the L-C dipole and the axisymmetrical vortex, with the initial vorticity distributions explained in the previous section. The time-dependent center postitions of the positive and negative vorticity parts of the L-C dipole ($\mathbf{r}_d^+(t)$ and $\mathbf{r}_d^-(t)$, respectively) are defined as

$$\mathbf{r}_d^\pm(t) \equiv \frac{\int_{A_d^\pm} (x,y)\,\tilde{\zeta}(x,y,t)\,dx\,dy}{\int_{A_d^\pm} \tilde{\zeta}(x,y,t)\,dx\,dy}\,, \tag{14}$$

where $A_d^\pm$ are the time-dependent regions of points (x,y,t) where $\pm\tilde{\zeta}(x,y,t) > 0$. The time-dependent center of the whole dipole $\mathbf{r}_d$ is given by

$$\mathbf{r}_d(t) \equiv \frac{\mathbf{r}_d^+(t) + \mathbf{r}_d^-(t)}{2}\,. \tag{15}$$

The time-dependent center position of the axisymmetrical vortex $\mathbf{r}_v(t)$ is defined in an analogous way to (14).

Initially the dipole moves with an almost straight trajectory approaching the axisymmetrical vortex (Figure 3). As the dipole gets closer to the target vortex, the dipole-vortex interaction increases due to the potential background-flows of both vortices. As a result of this interaction the dipole is attracted by the vortex and its trajectory acquires negative curvature (Figure 3). On the other hand, the axisymmetrical vortex is also attracted by the dipole's potential-flow, and is slightly accelerated towards the approaching dipole (Figure 3). The closer the vortices get, the dipole's speed of displacement decreases (Figure 4) due to the fact that the dipole poles open up relative to the dipole's axis (Figures 3 and 5). At the time of highest pole separation ($t \simeq 123$) the dipole's speed of displacement reaches a minimum (Figure 4) and the two centers of the vortices, as well as the centers of the poles, are completely alligned (Figure 3).

In this case, due to the large north-south initial distance between the dipole and the axisymmetrical vortex, there is no vorticity exchange between the vortices. After the time of largest interaction ($t \simeq 123$, Figure 5), the dipole's poles close and the dipole acquires a rigid vorticity distribution which is similar to its initial one but rotated positively (Figure 3).

The mechanism of the dipole's trajectory change, due to the interaction between the potential flows, involves a very small exchange of vorticity between the positive and negative poles and also in a small vorticity leakage, of both positive and negative vorticity, to the background field. While a L-C dipole consisting only on the first vorticity mode $\mathrm{J}_1(k_1 r)$, dipolar antisymmetrical mode, moves along a straight trajectory, the presence of the zero mode $\mathrm{J}_0(k_2 r)$, or rotational symmetrical mode, provides a constant curvature to the dipole's trajectory. In this numerical experiment the dipole, consisting initially of only the first vorticity mode $\mathrm{J}_1(k_1 r)$, develops a small rotational mode via vorticity exchange between the poles while approaching the axisymmetrical vortex. The direction of this vorticity exchange is reversed as the dipoles leaves the vortex, in such a way that the mode-0 vanishes and the poles recover their antisymmetrical vorticity distribution. On the other side, the axisymmetrical vortex decelerates towards a new position very close to its initial location (Figure 3). The whole interaction process is shown in the video referenced in Figure 6.

The dipole's speed of displacement after the interaction is very close to its original value (Figure 4). This interaction, practically involving no net vorticity change between initial and final dipole vorticity distributions, may be classified as an elastic scattering of a vortex dipole by an axisymmetrical vortex. Nevertheless, it is important to underline that changes in the initial vorticity distribution of the axisymmetrical

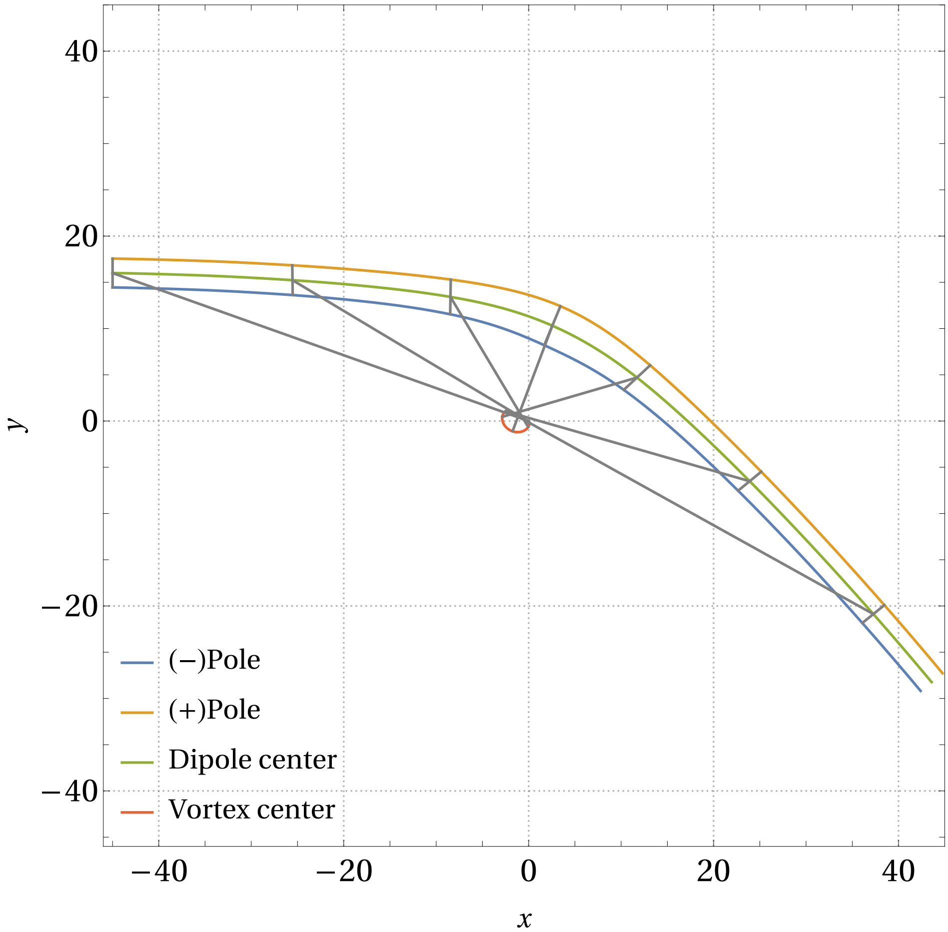

Figure 3. Trajectories of the center of the dipole poles $\mathbf{r}^{-}(t)$ (blue), $\mathbf{r}^{+}(t)$ (orange), the center of the whole dipole $\mathbf{r}_d(t)$ (green), and the center of the axisymmetrical vortex $\mathbf{r}_v(t)$ (red). The gray lines connect the + and − pole centers and the center of the dipole with the center of the vortex at seven different times.

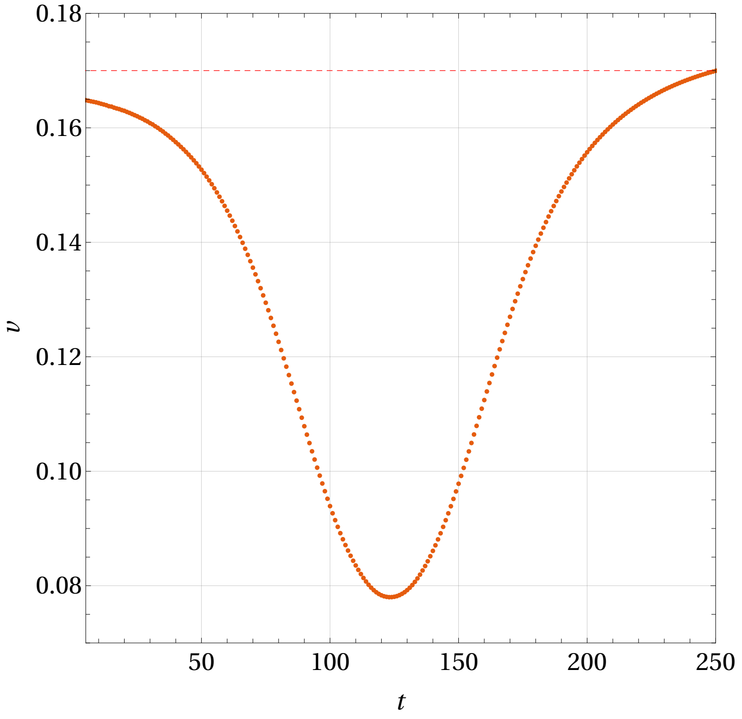

Figure 4. Dipole's speed of displacement $v_d(t) \equiv |d\mathbf{r}_d(t)/dt|$. The dashed red line marks the speed of displacement of the last point.

vortex this interaction may loose its elastic behaviour. For example, if the vortex vorticity boundary R_v is extended to the first zero $j_{1,1}/k_2$, in such a way that the vortex vorticity distribution is $\zeta(r)/C_v = \mathrm{J}_0(k_2 r) - \mathrm{J}_0(j_{1,1})$, so that there is no vorticity jump at the vortex boundary $\zeta(j_{1,1}/k_2) = 0$, the interaction is fully inelastic. In this case it occurs an exchange of the negative vorticity pole between the dipole and the axisymmetrical vortex. This example is described in more detail in Appendix B.

We have also analyzed interactions similar to the one described before but changing the initial positions of the dipole along the y-axis (video referenced in Figure 7). In this video, the dipole with green vorticity contours at the top simulates the elastic interaction described above. The dipole with black vorticity contours is located half the way of the green dipole. This interaction is really similar to the interaction described in Appendix B where the dipole is scattered by the axisymmetrical vortex and the dipole's poles separate. When the negative pole is close to the positive axisymmetrical vortex, these two vortices join together, giving rise to partner exchange and formation of a new dipole (video in Figure 7). The positive vorticity pole is left behind and evolves towards an axisymmetrical vortex close to the initial position of the initial axisymmetrical vortex.

The next dipole, with yellow vorticity contours, is located at the same y-coordinate as the axisymmetrical vortex ($y = 0$). In this case the vortices collide and merging occurs (video in Figure 7). The next two dipoles, with white and red vorticity contours, are situated at the same distance as the vortices black and green, respectively, but with reversed sign, so that the positive pole of the dipole is the closest pole to the axisymmetrical vortex. In these cases a positive-positive pole interaction occurs. The white dipole, closer to the axisymmetrical vortex, suffers straining out vorticity processes, while the red dipole, far from the axisymmetrical vortex, experiences also

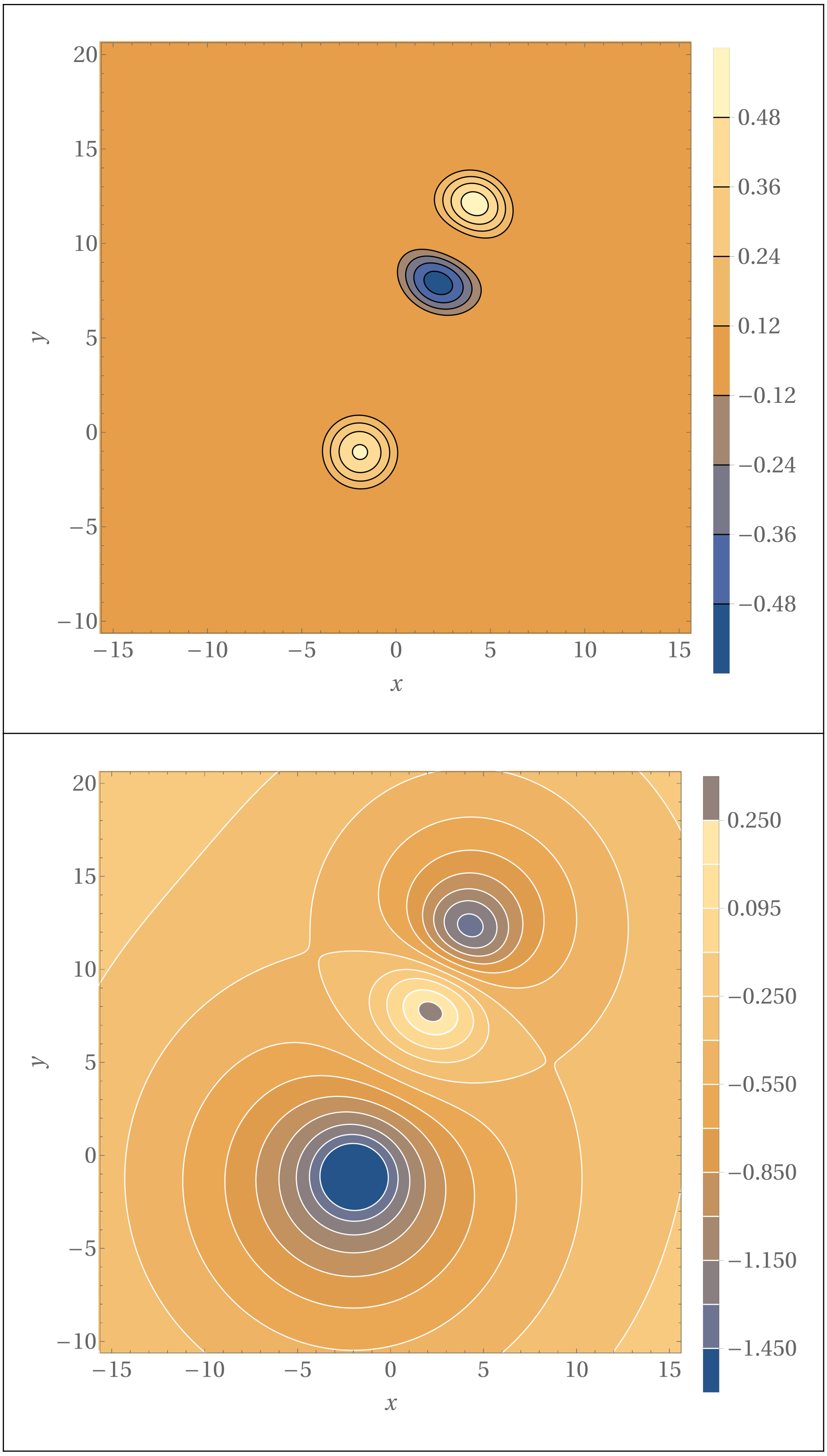

Figure 5. Vorticity (top) and stream function (bottom) distributions at the time of maximum poles separation ($t = 123$).

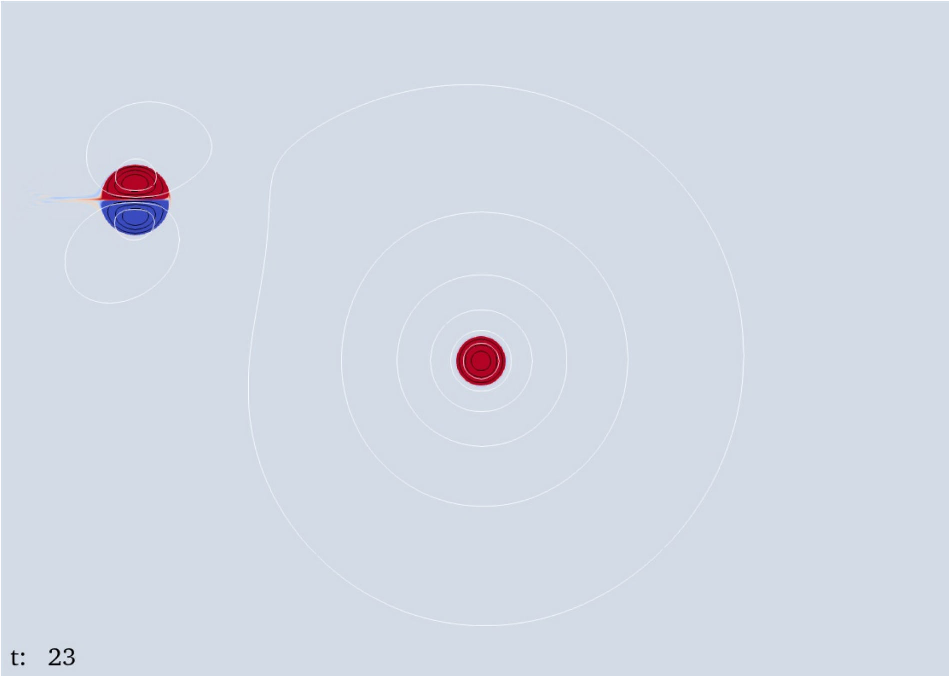

Figure 6. Video of the inelastic interaction between the dipole and the axissymmetrical vortex. The colour scale is saturated for a better visualization of the small vorticity changes. Blue and red colors mean negative and postiive vorticity, respectively. Vorticity contour lines (black) and stream function contour lines (white) are included.

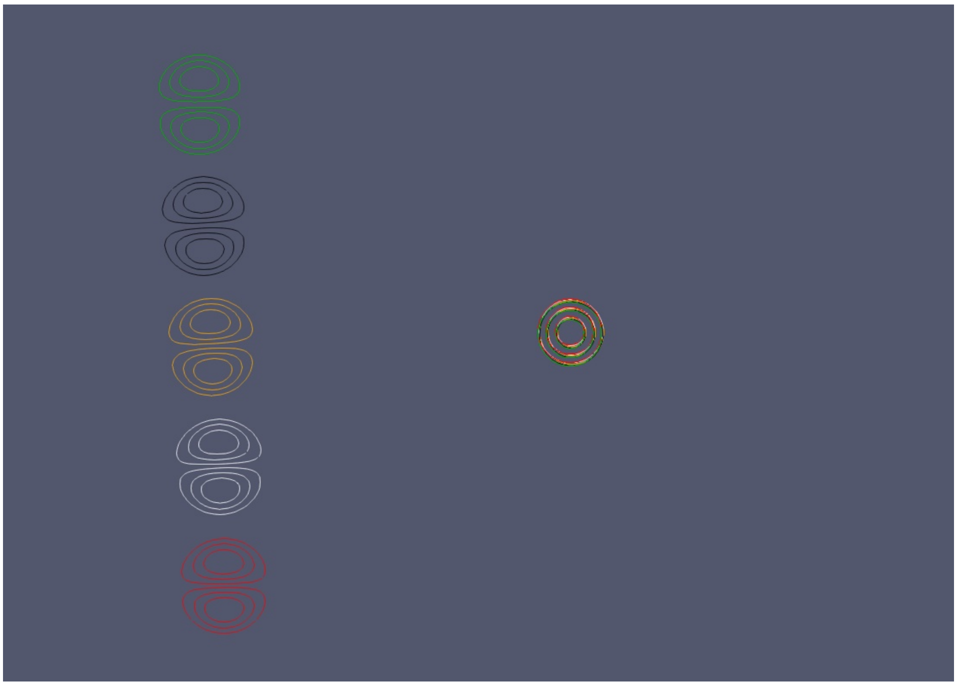

Figure 7. Superposition of five different simulations, represented with different vorticity contour line colors, of the interaction between the dipole and the axisymmetrical vortex. Each dipole starts at a different y-axis position. The axisymmetrical vortex is always placed at the position $(0, 0)$.

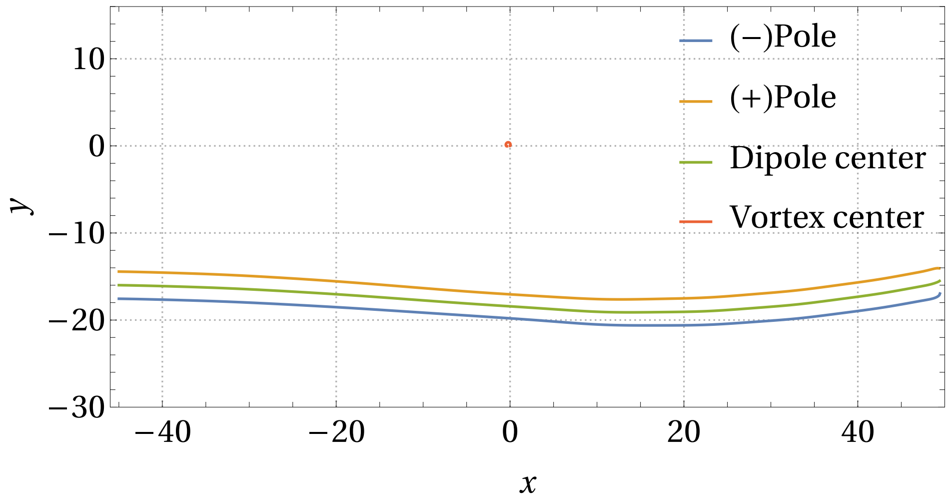

Figure 8. Trajectories of the center of the dipole poles $\mathbf{r}^-(t)$ (blue), $\mathbf{r}^+(t)$ (orange), the center of the whole dipole $\mathbf{r}_d(t)$ (green), and the center of the axisymmetrical vortex $\mathbf{r}_v(t)$ (red).

an elastic interaction but weaker than the one experienced by the green dipole (video in Figure 7). In this case the red dipole is slightly repelled, instead of being attracted, by the axisymmetrical vortex, in such a way that the dipole changes only slightly its direction during the interaction time, to afterwards return to a straight trajectory with the same initial direction. The axisymmetrical vortex behaves similar to the dipole, it is repelled by the potential flow of the dipole and describes an almost semi-circular trajectory with a small radius $\delta r \simeq 0.6$ (too small to be appreciated in Figure 8) and returns, after the interaction time, to a new location very close to the initial one.

Though this is a simple two-dimensional flow study, the application to three-dimensional balanced geophysical flows is straightforward under the quasi-geostrophic (QG) approximation. This is so because the two-dimensional initial vorticity conditions chosen are naturally applicable to the theory of baroclinic QG flows where the role played by the geopotential $\phi(\mathbf{x},t)$, horizontal geostrophic velocity $\mathbf{u}_h^g(\mathbf{x},t) \equiv \mathbf{k} \times \nabla\phi(\mathbf{x},t)$ and the materially conserved QG potential vorticity anomaly $\varpi^q(\mathbf{x},t) = \nabla^2\phi(\mathbf{x},t)$, in the three-dimensional QG space, is equivalent to the role played by the stream function $\psi(\mathbf{x}_h,t)$, horizontal velocity $\mathbf{u}_h(\mathbf{x}_h,t) \equiv \mathbf{k} \times \nabla\psi(\mathbf{x}_h,t)$ and the materially conserved vertical vorticity $\zeta(\mathbf{x}_h,t) = \nabla^2\psi(\mathbf{x}_h,t)$ in the 2D isochoric flows considered here. In three-dimensional QG flows, instead of the Bessel functions of the first kind $\mathrm{J}_n(r)$, which are the eigenfunctions of the radial part of the Laplacian operator in polar coordinates (r,θ), the relevant modes are the spherical Bessel functions of the first kind $\mathrm{j}_l(\rho)$ and the spherical harmonics $\mathrm{Y}_l^m(\vartheta,\varphi)$, of degree l and order m, which are the eigenfunctions of the radial part (ρ) and the angular part (ϑ,φ), respectively, of the Laplacian operator in spherical coordinates (ρ,ϑ,φ). This approach has been used recently to investigate three-dimensional baroclinic dipoles (Viúdez, 2019).

5 Concluding Remarks

In this work we have proved, using numerical simulations, that fully elastic interactions between a vortex dipole and an axisymmetrical vortex are possible in two-dimensional inviscid incompressible flows. In the particular example described in detail here, a Lamb-Chaplygin dipole is elastically scattered by an axisymmetrical vortex. When the initially straight moving L-C dipole approaches the target vortex they interact due to their corresponding potential flows, in such a way that the dipole's trajectory acquires curvature and the dipole's vorticity poles open up. Once the L-C dipole moves away from the target vortex, the dipole's poles close and the dipole continues with a straight trajectory but with a direction different from the initial one. No vorticity exchange between the dipole and the axisymmetrical vortex occurs, though there is a small vorticity exchange between the poles and a small vorticity leakage to the background field.

This description of an elastic interaction contributes to several previous studies involving dipoles interactions, including interactions of dipoles with solid boundaries (de Ruijter et al., 2004; Kloosterziel et al., 1993; Voropayev & Afanasyev, 1992; Zavala Sansón & Gonzalez, 2021), interactions of dipoles with inertia–gravity waves (Claret & Viúdez, 2010; Huang et al., 2017), and dipole-dipole interactions (Dubosq & Viúdez, 2007; McWilliams & Zabusky, 1982; Velasco Fuentes & Heijst, van, 1995; Voropayev & Afanasyev, 1992). In the cases of dipole-dipole and dipole-vortex interactions both elastic and inelastic processes are possible depending on the initial vorticity distribution, which includes the location, orientation and vorticity distributions of the vortices. In the main example shown in this work, due to the particular initial conditions chosen, inelastic interactions do not occur and the dipole-vortex interaction is practically elastic. We have also seen that a change in the vorticity distribution of the axisymmetrical vortex may lead to inelastic interactions involving vortex partner exchange.

The results shown in this work are applicable to three-dimensional baroclinic geophysical flows under the quasi-geostrophic (QG) approximation, as the initial vorticity distributions are based on the eigenfunctions of the two-dimensional Laplacian operator in circular geometry (the Bessel-azimuthal vorticity modes). Our future work is to investigate the stability of isolated geophysical vortices, including also vortex interactions, extending the approach of Viúdez (2021) in 2D to three-dimensional QG flows.

Appendix A Scheme of the Numerical Algorithm

Given an initial vorticity field $\zeta(x, y, t_0)$ the vorticity time integration is done in four steps.

1. The stream function $\psi(x, y, t_0)$ is obtained by solving (2) espectrally.
2. The velocity $\mathbf{u}(x, y, t_0)$ is computed from $\psi(x, y, t_0)$ using (1).
3. The vorticity advection $-\mathbf{u} \cdot \nabla\zeta$ is computed in the physical space.
4. The vorticity at the next time-step $\zeta(x, y, t_0 + \delta t)$ is obtained from (3) as

$$\zeta(x, y, t_0 + \delta t) = -\delta t\, \mathbf{u} \cdot \nabla\zeta + \zeta(x, y, t_0)\,.$$

After the step 4 the loop returns to step 1 for the next time integration $(t_0 + \delta t)$. The numerical simulations were carried out using a 2D pseudospectral code where the vorticity field $\zeta(x, y, t)$ is numerically integrated, following the steps described above, in a doubly periodic domain using an explicit leap-frog time-stepping method, together with a weak Robert-Asselin time filter to avoid the decoupling of even and odd time levels. The numerical domain was discretized in 2048^2 grid points.

Appendix B Dependence with the Radial Vorticity Profile of the Axisymmetrical Vortex

In this case the axisymmetrical vortex boundary R_v is extended to the first zero $R_v = j_{1,1}/k_2$, instead of $j_{0,1}/k_2$ (Figure 1), and its vorticity distribution is given by $\zeta(r)/C_v = \mathrm{J}_0(k_2 r) - \mathrm{J}_0(j_{1,1})$ so that $\zeta(j_{1,1}/k_2) = 0$ with no vorticity jump at the vortex boundary. The other initial conditions described in section 3 remain unchanged. In the general case where the vortex boundary is taken at $k_2 r = j_{m,n}$ the external flow $\mathbf{u}_0(r)$, is given by

$$\frac{\mathbf{u}_0(r)}{C_v/k_2} = \left[\frac{\mathrm{J}_0(j_{m,n})}{2} \frac{j_{m,n}^2}{k_2 r} - \mathrm{J}_1(j_{m,n}) \frac{j_{m,n}}{k_2 r} \right] \mathbf{e}_\theta \, .$$

If the vortex boundary is taken at $k_2 r = j_{1,1}$ the external flow decays as $C_v(\mathrm{J}_0(j_{1,1}) j_{1,1}^2/(2k_2^2 r)) \simeq -2.9/(k_2^2 r)$, while if the vortex boundary is taken at $k_2 r = j_{0,1}$, as in section 3, the external flow decays as $-C_v(\mathrm{J}_1(j_{0,1}) j_{0,1}/(k_2^2 r)) \simeq -1.2/(k_2^2 r)$, the ratio been $\mathrm{J}_0(j_{1,1}) j_{1,1}^2/(2\mathrm{J}_1(j_{0,1}) j_{0,1}) \simeq 2.4$, indicates that the external flow in this example decays faster than the exterior flow in section 3.

In this case, the dipole moves initially with a straight trajectory approaching the axisymmetrical vortex. Then, the vortices are attracted by their potential flows and the poles of the dipole separate. The difference with the case studied in section 3 is that, in this case, while the poles open up the axisymmetrical vortex is pushed away from the dipole, and the negative pole of the dipole separates from the positive pole and joins the axisymmetrical vortex, giving rise to a new dipole (Figure B1). The positive pole of the dipole is left behind and remains as an axisymmetrical vortex close to the position of the original one.

Acknowledgments
We acknowledge the Spanish Ministerio de Ciencia e Innovacin for the FPI Ph.D. grant (PRE2019-090309).

References

Afanasyev, Y. (2003). Spontaneous emission of gravity waves by interacting vortex dipoles in a stratified fluid: Laboratory experiments. *Geophysical & Astrophysical Fluid Dynamics*, *97*(2), 79-95. doi: 10.1080/0309192031000114349

Ahlnäs, K., Royer, T. C., & George, T. H. (1987). Multiple dipole eddies in the Alaska Coastal Current detected with Landsat thematic mapper data. *Journal of Geophysical Research: Oceans*, *92*(C12), 13041-13047. doi: https://doi.org/10.1029/JC092iC12p13041

Barton, E. D., Arístegui, J., Tett, P., & Navarro-Pérez, E. (2004). Variability in the Canary Islands area of filament-eddy exchanges. *Progress in Oceanography*, *62*(2), 71-94. (The Canary Islands Coastal Transition Zone - Upwelling, Eddies and Filaments) doi: https://doi.org/10.1016/j.pocean.2004.07.003

Besse, V., Leblond, H., Mihalache, D., & Malomed, B. (2014). Building patterns by traveling dipoles and vortices in two-dimensional periodic dissipative media. *Optics Communications*, *332*, 279-291. doi: https://doi.org/10.1016/j.optcom.2014.07.029

Carton, X. (2001, 05). Hydrodynamical modeling of oceanic vortices. *Surveys in Geophysics*, *22*, 179-263. doi: 10.1023/A:1013779219578

Chaplygin, S. (2007, 04). One case of vortex motion in fluid. *Regul. Chaot. Dyn.*, *12*, 219-232. doi: 10.1134/S1560354707020074

Claret, M., & Viúdez, A. (2010, 12). Vertical velocity in the interaction between inertia–gravity waves and submesoscale baroclinic vortical structures. *Journal of Geophysical Research (Oceans)*, *115*, C12060. doi: 10.1029/2009JC005921

Couder, Y., & Basdevant, C. (1986, 12). Experimental and numerical study of vortex couples in two-dimensional flows. *Journal of Fluid Mechanics*, *173*, 225-251. doi: 10.1017/S0022112086001155

de Ruijter, W. P., van Aken, H. M., Beier, E. J., Lutjeharms, J. R., Matano, R. P., & Schouten, M. W. (2004). Eddies and dipoles around South Madagascar: formation, pathways and large-scale impact. *Deep Sea Research Part I:*

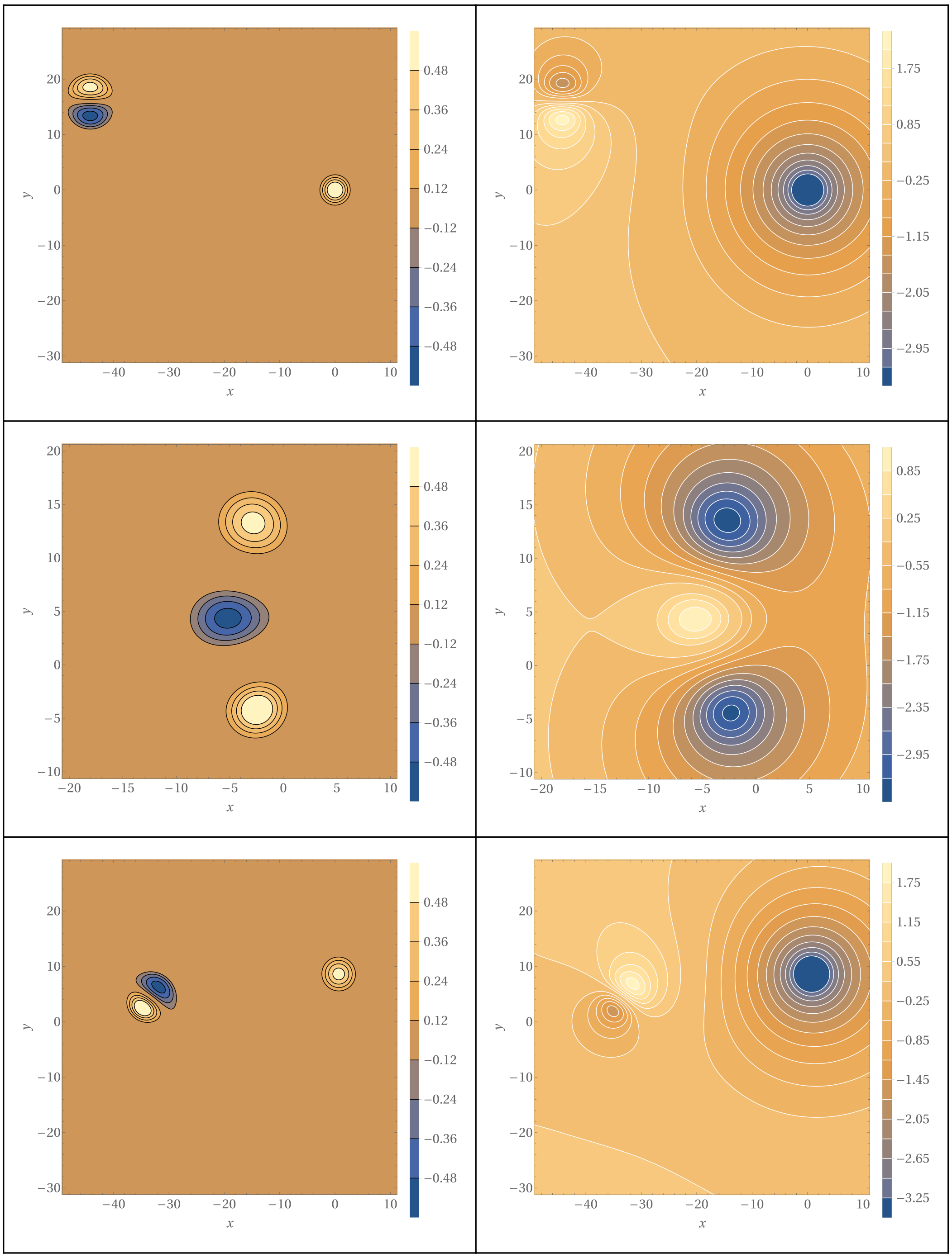

Figure B1. Time evolution of the vorticity (left) and stream function (right) of the inelastic interaction at times t=0 (top), t=70 (middle) and t=130 (bottom).

Oceanographic Research Papers, *51*(3), 383-400. doi: https://doi.org/10.1016/j.dsr.2003.10.011

Dritschel, D. G. (1995). A general theory for two-dimensional vortex interactions. *Journal of Fluid Mechanics*, *293*, 269303. doi: 10.1017/S0022112095001716

Dritschel, D. G., & Waugh, D. W. (1992). Quantification of the inelastic interaction of unequal vortices in two-dimensional vortex dynamics. *Physics of Fluids*, *4*, 1737-1744.

Dubosq, S., & Viúdez, A. (2007). Three-dimensional mesoscale dipole frontal collisions. *Journal of Physical Oceanography*, *37*(9), 2331-2344. doi: 10.1175/JPO3105.1

Flór, J. B., & Van Heijst, G. J. F. (1994). An experimental study of dipolar vortex structures in a stratified fluid. *Journal of Fluid Mechanics*, *279*, 101133. doi: 10.1017/S0022112094003836

Huang, X., Zhang, Z., Zhang, X., Qian, H., Zhao, W., & Tian, J. (2017). Impacts of a mesoscale eddy pair on internal solitary waves in the northern South China Sea revealed by mooring array observations. *Journal of Physical Oceanography*, *47*(7), 1539-1554.

Johannessen, J., Sandven, S., Lygre, K., Svendsen, E., & Johannessen, O. (1989, 01). Three-dimensional structure of mesoscale eddies in the Norwegian Coastal Current. *Journal of Physical Oceanography - J PHYS OCEANOGR*, *19*, 3-19. doi: 10.1175/1520-0485(1989)019⟨0003:TDSOME⟩2.0.CO;2

Kloosterziel, R. C., Carnevale, G. F., & Phillippe, D. (1993, 10). Propagation of barotropic dipoles over topography in a rotating tank. *Dynamics of Atmospheres and Oceans*, *19*(1), 65-100. doi: 10.1016/0377-0265(93)90032-3

Li, Z., Wang, X., Hu, J., Andutta, F. P., & Liu, Z. (2020). A study on an anticyclonic-cyclonic eddy pair off Fraser Island, Australia. *Frontiers in Marine Science*, *7*, 1061. doi: 10.3389/fmars.2020.594358

McWilliams, J. C., & Zabusky, N. J. (1982, 01). Interactions of isolated vortices I: Modons colliding with modons. *Geophysical and Astrophysical Fluid Dynamics*, *19*(3), 207-227. doi: 10.1080/03091928208208956

Rasmussen, J., Hesthaven, J., Lynov, J., Nielsen, A., & Schmidt, M. (1996). Dipolar vortices in two-dimensional flows. *Mathematics and Computers in Simulation*, *40*(3), 207-221. doi: https://doi.org/10.1016/0378-4754(95)00033-X

Ridderinkhof, W., Le Bars, D., von der Heydt, A. S., & de Ruijter, W. P. M. (2013). Dipoles of the south east Madagascar Current. *Geophysical Research Letters*, *40*(3), 558-562. doi: https://doi.org/10.1002/grl.50157

Santiago-García, M. W., Parés-Sierra, A. F., & Trasviña, A. (2019, 12). Dipole-wind interactions under gap wind jet conditions in the Gulf of Tehuantepec, Mexico: A surface drifter and satellite database analysis. *PLOS ONE*, *14*(12), 1-23. doi: 10.1371/journal.pone.0226366

Sheres, D., & Kenyon, K. E. (1989). A double vortex along the California coast. *Journal of Geophysical Research: Oceans*, *94*(C4), 4989-4997. doi: https://doi.org/10.1029/JC094iC04p04989

Velasco Fuentes, O., & Heijst, van, G. (1995). Collision of dipolar vortices on a beta-plane. *Physics of Fluids*, *7*(11), 2735–2750. doi: 10.1063/1.868652

Viúdez, A. (2019). Exact solutions of asymmetric baroclinic quasi-geostrophic dipoles with distributed potential vorticity. *Journal of Fluid Mechanics*, *868*, R1. doi: 10.1017/jfm.2019.234

Viúdez, A. (2021). Robust and unstable axisymmetric vortices, including neutral vortices, of a new two-dimensional vortex family. *Physics of Fluids*, *33*(5), 054103. doi: 10.1063/5.0048128

Voropayev, S. I., & Afanasyev, I. D. (1992, 03). Two-dimensional vortex-dipole interactions in a stratified fluid. *Journal of Fluid Mechanics*, *236*, 665-689. doi: 10.1017/S0022112092001575

Voropayev, S. I., & Afanasyev, Y. D. (1994). *Vortex structures in a stratified fluid.*

Chapman and Hall.
Wayne, C. E. (2011, 01). Vortices and two-dimensional fluid motion. *Notices of the American Mathematical Society*, *58*, 10-19.
Zavala Sansón, L., & Gonzalez, J. F. (2021). Travelling vortices over mountains and the long-term structure of the residual flow. *Journal of Fluid Mechanics*, *922*, A33. doi: 10.1017/jfm.2021.567